Comparing the Effects of Low-Protein and High-Carbohydrate Diets and Caloric Restriction on Brain Aging in Mice

Devin Wahl[1,2], **Samantha M. Solon-Biet**[1], **Qiao-Ping Wang**[1,3], **Jibran A. Wali**[1], **Tamara Pulpitel**[1], **Ximonie Clark**[1], **David Raubenheimer**[1], **Alistair M. Senior**[1,4], **David A. Sinclair**[5,6], **Gregory J. Cooney**[1], **Rafael de Cabo**[7], **Victoria C. Cogger**[1,2], **Stephen J. Simpson**[1,*], and **David G. Le Couteur**[1,2,8,*]

[1]Charles Perkins Centre, The University of Sydney, Sydney, NSW 2006, Australia

[2]Aging and Alzheimers Institute, ANZAC Research Institute, Centre for Education and Research on Ageing, Concord, NSW 2139, Australia

[3]School of Pharmaceutical Sciences (Shenzhen), Sun Yat-sen University, Guangzhou 510275, China

[4]School of Mathematics and Statistics, The University of Sydney, NSW 2006, Australia

[5]Department of Genetics, Paul F. Glenn Center for the Biology of Aging, Harvard Medical School, Boston, MA 02115, USA

[6]Department of Pharmacology, School of Medical Sciences, The University of New South Wales, Sydney, NSW 2052, Australia

[7]Translational Gerontology Branch, National Institute on Aging, NIH, Baltimore, MD 21224, USA

[8] Lead Contact

In Brief

Calorie restriction (CR) and *ad libitum* low-protein, high-carbohydrate (LPHC) diets improve cardiometabolic health in mice. Wahl et al. show that, like healthspan, CR and LPHC diets positively affect hippocampus biology in mice by influencing hippocampus gene expression, nutrient-sensing pathways, dendritic morphology, and cognition.

SUMMARY

Calorie restriction (CR) increases lifespan and improves brain health in mice. *Ad libitum* low-protein, highcarbohydrate (LPHC) diets also extend lifespan, but it is not known whether they are

beneficial for brain health. We compared hippocampus biology and memory in mice subjected to 20% CR or provided *ad libitum* access to one of three LPHC diets or to a control diet. Patterns of RNA expression in the hippocampus of 15-month-old mice were similar between mice fed CR and LPHC diets when we looked at genes associated with longevity, cytokines, and dendrite morphogenesis. Nutrient-sensing proteins, including SIRT1, mTOR, and PGC1α, were also influenced by diet; however, the effects varied by sex. CR and LPHC diets were associated with increased dendritic spines in dentate gyrus neurons. Mice fed CR and LPHC diets had modest improvements in the Barnes maze and novel object recognition. LPHC diets recapitulate some of the benefits of CR on brain aging.

Graphical Abstract
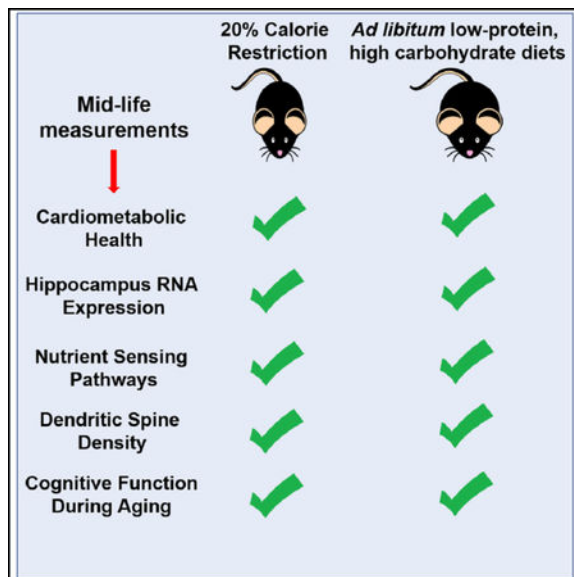
INTRODUCTION

Nutritional interventions, such as caloric restriction (CR), influence aging and age-related changes in the brain (Mattson et al., 2018; Wahl et al., 2016). CR improves cognitive function, including learning and memory, in old rodents (Ingram et al., 1987; Wahl et al., 2017), possibly mediated by its effects on cardiometabolic risk factors, generic hallmarks of aging, specific brain-related mechanisms (BDNF, neurogenesis) or nutrient-sensing pathways (Wahl et al., 2016).

CR is not readily translatable in humans. Therefore, other interventions that recapitulate the benefits of CR on brain function without the requirement for long-term reduction in food intake are being explored. Recently, we utilized the geometric framework (Simpson and Raubenheimer, 2012) to evaluate the effects of *ad libitum*-fed diets varying in macronutrients and energy content on aging. Mice consuming a low-protein, high-carbohydrate, low-fat diet (LPHC, protein:carbohydrate ~1:10) lived longest and were healthier in old age, even when compared to CR achieved by dilution of chow with non-digestible fiber (Solon-Biet et al., 2014). The beneficial effects of LPHC diets on lifespan

are conserved across a range of organisms from invertebrates to mice (Le Couteur et al., 2016).

The effects of LPHC diets on brain aging are unknown. However, the observation that *ad libitum*-fed LPHC diets are beneficial for lifespan and late-in-life cardiometabolic health suggest that they may also delay brain aging. To test this hypothesis, we evaluated the effects of four *ad-libitum*-fed diets varying in protein and carbohydrates and compared them to a standard 20% CR regimen in mice. Metabolic phenotype and markers of cognitive function and underlying neurobiological processes were investigated with a focus on the hippocampus. Despite differences in aspects of metabolic phenotype, *ad libitum* LPHC diets conferred benefits to the hippocampus that are similar to standard 20% CR.

RESULTS

Cardiometabolic Parameters and Body Composition

Systemic parameters were determined at 15 months of age in mice fed one of five diets from weaning; diets are shown in Table 1. Daily energy intake, which rose with dilution of dietary protein by carbohydrate, was maximal on the 5% protein diet (Figures 1A and1B), consistent with protein leverage (Sørensen et al., 2008). Overall, CR and/or 5% protein diets were associated with lower body fat and weight, glucose tolerance, insulin, and leptin and higher adiponectin and FGF-21 (Figures 1C and 1K). These diets had no significant effect on insulin-like growth factor 1 (IGF-1) (Figure 1I), whereas cholesterol was highest on the 10% protein diet and lowest with CR (Figure 1L). There were some differences between male and female mice as shown. Other differences found included: urea, albumin, alanine transaminase and the exchange ratio of CO_2 and O_2 (respiratory quotient, RQ) (Table S1).

Hippocampal Gene Expression

Hierarchical clustering of differentially expressed genes from total hippocampus tissue revealed differences between the dietary groups as visualized with a heatmap (Figure 2A). Principle component analysis did not reveal differences between sexes (data not shown) and were therefore combined. CR had a marked effect on gene expression compared to control diet, while LPHC diets were associated with intermediate patterns of expression. The top-10 differentially expressed genes are listed in Table S2. Protein-Coupled Receptor 17 (*Gpr17*) is the top upregulated gene for all LPHC diets. CR was associated with altered expression of genes associated with circadian rhythm (*Dbp*) (Nikonova et al., 2017) and neuronal proliferation (*Dchs1*) (Beste et al., 2016).

FPKM (fragments per kilobase of transcript per million mapped reads) values were used to construct a volcano plot for gene expression that correlated with protein intake (Figure 2B; Table S3). The top gene positively correlated with protein intake was Gamma-aminobutyric acid type A receptor beta 2 subunit (*Gabrb2*), that encodes $GABA_A$ receptors. The top gene negatively correlated with protein intake was Zinc-Finger CCCH-Type-Containing 13 (*Zc3h13*), which is involved in nuclear factor kB (NF-kB) production (Gewurz et al., 2012).

Overlap of genes influenced by CR or correlated with protein intake was determined (Figure 2C). Compared to expression with control diet, CR was associated with 237 genes that were

upregulated and 238 genes that were downregulated. There were 379 genes that were upregulated with lower protein (and higher carbohydrate) intake and 438 genes that were downregulated with lower protein (and higher carbohydrate) intake. Only 40 overexpressed genes and 34 underexpressed genes were shared between CR and lower protein intake (Table S4), and several of these were of interest, including Semaphorin 4B (*Sema4b*), which is involved in synapse formation (Paradis et al., 2007), and Carboxypeptidase E (*Cpe*), which is a trophic factor that might influence neuron survival during aging (Cheng et al., 2014).

The effects of diets on biological pathways were determined (Figure 2D; Table S5). Pathways influenced by diet included several brain-specific and general cellular processes; surprisingly few overlapping pathways were among the groups. However, dendrite morphogenesis, synapse functioning, and neuronal development pathways were influenced by CR and dietary protein.

The changes in gene expression induced by the different diets were compared to genes that are reported to influence aging in mice (GenAge: The Aging Gene Database [http://genomics.senescence.info/genes/]) (Figures 2E and 2F; Tables S6 and S7). The patterns of expression (determined by log2fold change compared with 19% protein diet) with LPHC and CR diets were similar when categorized by genes that shorten lifespan (''Antilongevity'' genes) and those that extend lifespan (''pro-longevity'' genes). CR and LPHC diets upregulated and downregulated both anti-longevity and pro-longevity genes in variable patterns.

Hippocampal Nutrient-Sensing Pathway Proteins

CR elicits beneficial responses in the hippocampus via expression of nutrient-sensing proteins (Pani, 2015), including SIRT1, PGC1α, and MTOR. We found significant sex differences in the hippocampal expression of these proteins. In female mice SIRT1 protein expression was greatest in CR and 5% protein diets while in male mice there were no effect of diet (Figure 3A). In female mice MTOR activation (p-MTOR/MTOR) was lowest with CR and lowest protein diets (Figure 3B) and there was a positive correlation with MTOR activation and protein intake (and a negative correlation with carbohydrate intake) in both male and female mice (Figure S2A). PGC1α protein expression was increased only in male mice on CR (Figure 3C).

The top genes that are consistently upregulated (Figure 3D) and downregulated (Figure 3E) with CR from a recent meta-analysis (Plank et al., 2012) were compared with their expression in this study. CR and LPHC had similar effects on the patterns of expression. Several genes of interest, including Carbonyl reductase 1 (*Cbr1*), contribute to protection against oxidative damage and ischemia (Kim et al., 2014) (Figures 3D and 3E; Table S8).

Hippocampal Markers of Neuroinflammation

Pro-inflammatory cytokines interleukin (IL)-6 and tumor necrosis factor alpha (TNF-α), the anti-inflammatory cytokine IL-10 and brain-derived neurotrophic factor (BDNF) were measured. There was an increase in hippocampus IL-10 in lowest protein and CR diets (Figure S1A) but no changes in TNF-α, IL6, or BDNF (Figures S1B, S1C, and S1F). There were no significant differences among the groups in the number of hippocampus Iba1^{+} cells

(Figure S1D and S1E). Next, we looked at total hippocampus GFAP expression as measured by immunofluorescence but were not able to detect any differences among the groups (Figure S1G; Table S9).

Changes in gene expression were compared to those reported to influence cytokine response (AmiGO online gene ontology database: http://amigo.geneontology.org/amigo) (Figure S1H; Table S9). The patterns of expression with LPHC and CR diets were similar in terms of their effect on genes influencing cytokine response. A gene of interest was Suppressor of Cytokine 1 (*Socs1*), which is involved in suppressing brain inflammation (Walker et al., 2015).

Dendritic Spine Density in the Hippocampus Dentate Gyrus

The lowest protein and CR groups had increased dendrite spine density in the dentate gyrus (Figures 4A and 4B). However, the protein expression of drebrin, which is involved in the maintenance and formation of dendritic spines, was unchanged (Figure S2B).

The changes in gene expression induced by diet were compared to genes that are reported to influence dendrite morphogenesis (AmiGO online gene ontology database: http://amigo.geneontology.org/amigo) (Figure 4C; Table S10). The patterns of expression with LPHC and CR diets showed increasing upregulation of these genes as protein content of the diet decreased and with CR.

Memory and Learning in Middle-Aged and Old Mice

The Barnes maze and novel object recognition tests were used to assess the effects of diet on memory and learning at 13 and 23 months of age. Overall, changes in some parameters tended to show a benefit for CR and lower protein diets primarily in female mice.

In 13-month-old females, CR was associated with best performance on the Barnes maze on days 1 and 2, whereas, in 23-month-old females, CR was associated with best performance on day 4. The lower protein diets were also associated with some trends suggestive of improvement, with the 15% protein diet having the best performance on day 3 in the 13-month-old female mice and the 10% protein diet having the best performance on day 3 in the 23-month-old female mice (Figures 5A and 5B). In male mice, the only significant finding was that the 13-month-old mice on 10% protein diets performed best on days 2 and 3 (Figures 5C and 5D).

The significant findings for the novel object recognition test were that the 13-month-old female mice on the CR and 10% protein diets had the best recognition indices (Figure 5E). Interestingly, there was a negative correlation with body fat at young age and subsequent old-age recognition index scores (Figure 5G).

DISCUSSION

Aging is a powerful risk factor for the development of many diseases, particularly dementia. Identifying nutritional interventions that delay brain aging and can be easily implemented in humans is especially important because no pharmacological treatments have been

discovered that maintain brain function or reduce the risk of dementia. In this study, the effects of *ad libitum* LPHC diets on brain aging were studied and compared with standard CR.

Studies of CR and protein restriction on brain health and neurodegenerative disease in aging rodents have usually shown positive outcomes (Ingram et al., 1987; Mattson, 2010; Newman et al., 2017; Pani, 2015; Parrella et al., 2013). In our study, CR diets and LPHC diets were associated with modest improvements in behavioral and cognitive outcomes, although the results were mainly limited to females and inconsistent. Of note, the standard chow diet did not perform best for any measurement at any time point or for either sex. The results provide some support for the conclusion that CR and possibly LPHC diets improve brain function in old age.

CR and LPHC diets had marked effects on systemic cardiometabolic outcomes, which are increasingly recognized as risk factors for cognitive impairment and the risk of neurodegenerative disease (Buffa et al., 2014; Dye et al., 2017). These results are consistent with other studies of CR and LPHC diets (Simpson et al., 2017; Solon-Biet et al., 2015; Testa et al., 2014). FGF-21, a hormone linked with cardiometabolic health, was elevated in the 5% protein group, confirming our previous conclusion that FGF-21 is driven by low dietary protein coupled with elevated carbohydrate intake (Solon-Biet et al., 2016). Midlife body fat in females was correlated with novel object recognition in old mice, which parallels human observational studies linking midlife obesity with subsequent risk of dementia (Tolppanen et al., 2014).

We examined the effects of CR and LPHC diets on hippocampal gene expression. Other studies have reported changes in hippocampal gene expression with food restriction (Wood et al., 2015), influencing age-dependent changes in gene expression (Prolla and Mattson, 2001; Schafer et al., 2015), including genes involved with oxidative stress (Schafer et al., 2015) mitochondrial function and synaptic plasticity (Zeier et al., 2011). Overall, we found that gene expression signatures in CR and LPHC diets were different; however, there were similarities when specific genes involved with brain aging were analyzed, such as prolongevity genes, antilongevity genes, and genes involved with CR, inflammation, and dendrite morphogenesis.

The top upregulated gene for all three LPHC groups was the G-protein-coupled receptor, *Gpr17*. *Gpr17* is widely expressed in the brain, particularly in neuroprogenitor cells and contributes to myelination of axons and neuronal repair after acute injury (Alavi et al., 2018). Intriguingly *Gpr17* also has been found to be involved with food intake; knockout of *Gpr17* reduced food consumption in mice (Ren et al., 2012). Our data suggest that *Gpr17* expression responds to dietary macronutrient balance, which provides a mechanistic link between diet and brain aging.

The beneficial effects of CR on aging are in part mediated by its impact on several nutrient-sensing pathways such as SIRT1, MTOR, and PGC1α (Hadem et al., 2017), which also have been linked with brain aging (Mazucanti et al., 2015). We found that SIRT1 and MTOR were influenced by CR and dietary P:C only in female mice, while PGC1α was markedly

increased in males with CR. Our results are consistent with other studies showing a sex-specific effect of CR on nutrient-sensing path-ways and outcomes (Mitchell et al., 2016).

CR has been reported to reduce pro-inflammatory cytokines, increase anti-inflammatory cytokines (Willette et al., 2013) and increase BDNF in the hippocampus (Stranahan et al., 2009). We found that CR and LPHC were associated with increased levels of the anti-inflammatory cytokine IL-10, which influences brain response to acute injury (Garcia et al., 2017), while IL-10 in macrophages decreases with age and impairs recovery from neural injury (Zhang et al., 2015). We couldn't detect any effect of nutrition on other inflammatory cytokines, including IL6 and TNFα or the neurotrophic cytokine, BDNF. Increased expression of glial fibrillary acidic protein (GFAP) has been linked with inflammation, astroglial activation, and gliosis during brain degeneration (Brahmachari et al., 2006). Therefore, we investigated the effects of the nutritional interventions on total GFAP immunofluorescence expression in the hippocampus. We were not able to detect any changes among the groups in GFAP expression, suggesting that the dietary interventions in the current study did not influence neuroinflammatory processes that have been associated with neurodegenerative disease.

The dentate gyrus (DG) of the hippocampus contributes to the consolidation and formation of spatial memory, and dendritic spines in the DG are important for optimal neuronal function and the formation of memories (Kesner, 2017). CR has been reported to increase DG dendritic spine density in a mouse model of diabetes (Stranahan et al., 2009). We found that both CR and 5% protein diets increased dendritic spine density, consistent with the role of dendritic spines in cognitive and behavioral outcomes and the response to dietary interventions.

We recognize limitations to the current study. First, analyses of the hippocampus and metabolic data were acquired at only one time point, 15 months, which represents late midlife, although our behavioral evaluation included 23-month-old mice. Future research should focus on older mice and models of neurodegenerative disease. We studied dendritic spine counts in the dentate gyrus because of its critical role in hippocampus-dependent brain function (Toda and Gage, 2017), but not other areas involved in memory formation (CA1 or CA3).

In conclusion, both CR and LPHC diets impacted on brain aging in the hippocampus. Although the behavioral and cognitive changes were subtle, there were more dramatic effects on gene expression, protein activity, and dendritic spine morphology. Overall, the lowest protein, highest carbohydrate diets (5% and 10% protein) generated changes, which approached those seen with CR. A very low-protein, high-carbohydrate diet may be a feasible nutritional intervention to delay brain aging.

STAR★METHODS

KEY RESOURCES TABLE

REAGENT or RESOURCE	SOURCE	IDENTIFIER
Antibodies		
Phospho-mTOR (Ser2448) Antibody	Cell Signaling Technology	#2971; RRID:AB_330970
mTOR (7C10) Rabbit mAb	Cell Signaling Technology	#2983; RRID:AB_2105622
SirT1 (D1D7) Rabbit mAb	Cell Signaling Technology	#9475; RRID:AB_2617130
β-Actin (13E5) Rabbit mAb	Cell Signaling Technology	#4970; RRID:AB_2223172
Anti-Drebrin antibody	abcam	ab60933; RRID:AB_10675963
Anti-GAPDH antibody - Loading Control	abcam	ab9485; RRID:AB_307275
Anti-PGC1 alpha antibody	abcam	ab54481; RRID:AB_881987
Anti-rabbit IgG, HRP-linked Antibody	Cell Signaling Technology	#7074; RRID:AB_2099233
Rabbit Polyclonal Anti-Iba1 antibody	GeneTex	GTX100042; RRID:AB_1240434
Rabbit Polyclonal Anti-GFAP antibody	Abcam	ab7260; RRID:AB_305808
Goat anit-Rabbit IgG (H+L) Cross-Adsorbed Secondary Antibody, Cyanine3	ThermoFisher Scientific	A10520; RRID:AB_2534029
VECTASHIELD Antifade Mounting Medium with DAPI	Vector Laboratories	H-1200; RRID:AB_2336790
Chemicals, Peptides, and Recombinant Proteins		
DPX Mounting Media for histology	Sigma-Aldrich	06522
cOmplete, EDTA-free Protease Inhibitor Cocktail	Sigma-Aldrich	COEDTAF-RO ROCHE
10x Tris Buffered Saline (TBS)	Bio-Rad	#1706435
TRI Reagent® for DNA, RNA and protein isolation	Sigma-Aldrich	93289
Ponceau S Dye	Sigma-Aldrich	P7170
Critical Commercial Assays		
FD Rapid GolgiStain Kit (large)	FD Neurotechnologies	PK401
BDNF E_{max}® ImmunoAssay Systems	Promega	G7610
MCYTOMAG-70K j MILLIPLEX MAP Mouse Cytokine/Chemokine Magnetic Bead Panel - Immunology Multiplex Assay	Merck Millipore	# MCYTOMAG
Pierce BCA Protein Assay Kit	Thermo Fisher Scientific	23225
Mouse Leptin ELISA Kit	Crystal Chem High Performance Assays	90030
Mouse Adiponectin ELISA Kit	Crystal Chem High Performance Assays	80569
Fibroblast Growth Factor 21 Mouse/Rat ELISA	BioVendor Research and Diagnostic Products	RD291108200R
Ultra Sensitive Mouse Insulin ELISA Kit	Crystal Chem High Performance Assays	90080
Deposited Data		

REAGENT or RESOURCE	SOURCE	IDENTIFIER
Raw sequence data deposited into NCBI	Total Hippocampus RNA	GEO: GSE111778
Experimental Models: Organisms/Strains		
C57/b6 male and female mice	Animal Resource Centre, Perth, WA	N/A
Software and Algorithms		
NeuronStudio	Mount Sanai School of Medicine, freely available available online	http://research.mssm.edu/cnic/tools-ns.html
ImageJ	National Institutes of Health, freely available online	https://imagej.nih.gov/ij/
AnyMaze behavioral tracking software	Stoelting Co. Wood Dale, IL.	http://www.anymaze.co.uk/
The R Project for statistical computing	Freely available online	https://www.r-project.org/
GraphPad Prism Software	Available for download online	https://www.graphpad.com/scientific-software/prism/

CONTACT FOR REAGENT AND RESOURCE SHARING

Further information and requests for resources and reagents should be directed to and will be fulfilled by the Lead Contact, Professor David G. Le Couteur (david.lecouteur@sydney.edu.au).

EXPERIMENTAL MODEL AND SUBJECT DETAILS

Animal husbandry and diets—Animals were purchased from the Animal Resource Centre (Perth, WA) and housed four per cage on a 12-hour light/dark cycle at 22–24°C at the Charles Perkins Centre at The University of Sydney. All animals were given free access to water and randomly assigned to experimental groups. *Ad-libitum* animals were given free-access to food while CR animals were given an allotment with 20% fewer calories than the average intake of their *ad-libitum* 19% protein counterparts daily at 3.00pm. Mice were weaned at 3 weeks of age and diets were started at approximately three months of age. Energy intake from each macronutrient was determined and averaged daily from 12 – 15 months of age. Body weights were taken every two weeks and animals were routinely monitored every week for general health. The ethics in this study were approved by the University of Sydney, animal ethics number 2014/752.

Diets were purchased from Specialty Feeds (Perth, Western Australia) and formulated to have the same total energy content (isocaloric) but different ratios in protein to carbohydrate with fixed fat (Table 1). Each diet was based on the rodent diet AIN-93G (Specialty Feeds) and formulated to contain all essential vitamins, minerals, and amino acids for growth in mice. The primary dietary protein component was casein, the main carbohydrate component was starch, and the main fat component was soy oil.

METHOD DETAILS

Animal sacrifice and tissue collection—At 15 months of age a subset (n = 12 males, n = 12 females per group) of mice were culled. All animals were sacrificed between the hours of 10am and 12 noon. Animals were sacrificed in randomized order to minimize experimental bias. After deep anesthetizing with xylazine-ketamine (10mg/g bw), approximately 1 mL of blood was taken via cardiac puncture. The liver was removed, weighed, and flash-frozen in liquid nitrogen. The mice were then decapitated and the brain was carefully removed. One-half of the brain was immediately washed with ice-cold double-deionized water and placed into Golgi-Cox solution. The whole hippocampus was carefully dissected from the other half, immediately snap-frozen in liquid-nitrogen, and moved to -80^OC until further processing. The blood was placed into a ice-cold tube and placed directly into wet ice before centrifugation at 14,000 rpm for 10 minutes for plasma collection. The plasma was used for subsequent metabolic and systemic measurements. Males and females were analyzed separately on metabolic measurements due to innate metabolic differences between sexes (Valencak et al., 2017).

Fat mass and lean mass—Fat mass and lean mass were measured by magnetic resonance imaging (EchoMRI 900 – EchoMRI LLC, Houston, Texas, USA). The mice were awake during the process and snuggly put into a plastic tube before being placed inside the machine for approximately 1 minute. The machine calculated the fat mass (g) and lean mass (g) per each mouse.

Metabolic measurements—The respiratory quotient was measured by Metabolic Cage (Promethion, Sable Systems International, Las Vegas, NV, USA). Briefly, individual mice were placed in each cage and acclimatized for 8 hours then left for 48 hours (2 dark and 2 light cycles). Calorimetric data were calculated with the software and the average respiratory quotient was obtained during the dark cycle. Data are presented as CO_2 eliminated/O_2 consumed (Respiratory quotient; RQ).

Glucose tolerance—Glucose tolerance was measured at 15 months of age. Mice were fasted for 6 hours before the test which took place in the afternoon at 2.00 pm. Mice were orally gavaged with glucose (2 g/kg lean mass) and blood glucose levels were read by tail snip at time 0, 15 min, 30 min, 45 minutes, 60 minutes, and 90 minutes (Accu-Check Performa, Roche, Australia). The total area under the curve (AUC) was calculated and data are presented as mm/l.min.

Insulin determination—Total fasting insulin levels were measured with an ultra-sensitive mouse insulin ELISA kit per manufacturer's instructions (Chrystal Chem, Elk Grove Village, IL, USA). Whole blood was added to each well in the 96-well plate containing 90 μL of the provided diluent "G." 10 μL of blood was collected by tail snip and added to each well. The "mouse insulin standard" was reconstituted and the standards were mixed (from 0.1 ng/μL to 6.4 ng/μL). 95 μL of the provided diluent and 5 ml of each standard was added into each well, the plate was covered, and incubated overnight at 4°C. The plate was removed from 4^OC and washed 5 times with 250 ml wash buffer and 100 ml of the anti-inulin conjugate was added to each well. The plate was covered and incubated for 30

minutes at room temperature and subsequently washed 7 times with 250 μL wash buffer in each well. 100 ml of the enzyme substrate was added to each well, covered in the dark for 40 minutes, and the reaction ended with the addition of 100 ml stop solution ''F.'' The plate was read at an absorbance of A450-A630 and insulin concentration was determined by linear fit. Data are presented as ng/μL.

FGF-21 assay—The Fibroblast Growth Factor-21 assay was analyzed by ELISA (Biovendor, Karasek, Czech Republic). The mouse master standards were reconstituted with the provided dilution buffer (40 pg/μL – 2568 pg/mμL). 100 ml of standards and diluted samples (serum diluted in dilution buffer) were added to each appropriate well. The plate was incubated at room temperature for one hour with shaking at 300 rpm and washed three times with the provided wash buffer. 100 ul of biotin-labeled antibody was subsequently added to each well and incubated for one hour at room temperature with shaking. The wells were washed 3x with the wash buffer and 100 μL of Sterptavidin-HRP conjugate was added to each well and incubated with shaking for 30 minutes. The plate was washed 3x with wash buffer and 100 ml of substrate solution was added to each well, covered in foil, and incubated at room temperature for 10 minutes, and the reaction was stopped by the addition of 100 ml of stop solution. The absorbance of each well was determined by reading on a microplate reader at 550 – 650 nm and concentrations were determined with the standard curve. Data are presented serum FGF-21 concentration in pg/μL.

Adiponectin determination—Adiponectin concentrations were determined using a mouse adiponectin ELISA kit (Crystal Chem, Elk Grove Village, Il, USA). The mouse standards were reconstructed from the provided stock (0.025 – 1 ng/μL). Serum samples were diluted to the appropriate concentration (1:10,000) in the dilution buffer. 100 μL of sample and each standard were added to each well and incubated for 1 hour at RT with shaking for 350 RPM. The plate was washed 3x and 100ul of the provided antibody conjugate was added to each well and incubated for 1 hour with shaking at 350 rpm. The plate was washed 3x with wash buffer, 100 μL of substrate solution was added and incubated for 30 minutes. 100 μL of stop solution was added and the OD was measured at 460/630 nm. Data are presented as the Adiponectin concentration in ng/μL.

Leptin determination—Leptin concentrations were determined using a mouse leptin ELISA kit (Crystal Chem, Elk Grove Village, Il, USA). The mouse standards were reconstructed from the provided stock (0.0 – 12.8 ng/μL) and serum samples were diluted to the appropriate concentrations. 100 μL of each standard or sample was added to each well and incubated overnight at 4°C. The plate was then washed and 100 μL of the conjugate solution was added followed by 4 hours of incubation at 4°C. The plate was washed and 100 μL of the substrate solution was added, incubated for 30 minutes, and 100 μL of stop solution was added to each well. The plate was read on a spectrometer at an OD of 450/630 nm. Data are presented as serum leptin levels in ng/μL.

Cholesterol, Albumin, ALT, Urea, and Triglycerides—Serum cholesterol, albumin, ALT, urea, and triglyceride levels were analyzed by a Cobas 8000, c702 photometric module

(Hitachi, Japan) and all reagents were provided by Roche (Roche diagnostics, Germany). All analyses were completed at Concord Hospital (NSW, Australia).

RNA isolation and processing—RNA was isolated using the *Trizol* method. 1μL of ice-cold TRIzol reagent (Sigma Aldrich, St. Louis, MO, USA) was added to fresh frozen whole hippocampus. Tissue was homogenized using the bead method (QIAGEN, Hilden, Germany) for 30 s at 50 *Hz*. After samples were let to sit on ice for 10 minutes, 200 ml of ice-cold chloroform was added and samples were let to sit at room temperature for an additional 3 minutes. Samples were centrifuged at 14,000 rpm for 20 minutes and approximately 500 μL of the supernatant was collected and added to an equal volume of ice-cold 2-propanol. Samples were mixed, placed directly on ice, and centrifuged at 14,000 RPM for 20 minutes. The supernatant was removed and the remaining pellet was washed with 500 μL of ice-cold ethanol 3 times before air-drying. The pellet was resuspended in 15 μL nuclease-free water and cleaned with DNase (Invitrogen, Carlsbad, CA, USA). RNA purity was assessed using a nanodrop spectrometer (Thermofisher Scientific Australia) before freezing at —80°C until further analysis.

RNA sequencing and analysis—Samples were processed by The Australian Genome Research Facility (AGRF - Victoria, Australia; http://www.agrf.org.au/) with Illumina TruSeq stranded mRNA sample preparation and technology. RNA integrity was initially assessed by a bioanalyzer and all samples passed quality control with RIN values ≥ 8.0 and an A260/280 ratio of 1.8 – 2.0. Briefly, mRNA was purified via oligo(dT) beads followed by fragmentation of mRNA with divalent cations and heat. 1st strand cDNA synthesis was randomly primed followed by second strand cDNA synthesis. cDNA library preparation was prepared first by DNA fragment end repair followed by 3' adenylation of DNA fragments and subsequent sequencing adaptor ligation. Finally, the library was amplified by PCR.

Primary sequence data were generated using the Illumina bcl2fastq 2.19.0.12 pipeline and sequence reads from all samples were analyzed per AGRF quality control measures. Briefly, cleaned sequence reads were aligned against the *Mus musculus* genome (Build version mm10). The Tophat aligner (v2.0.14) was used to map reads to the genomic sequences. The raw gene reads were generated by featureCounts (v1.4.6) and the differential gene expression was analyzed by DESeq2 (v1.16.1) in R (package v3.4.0). The Gene Set Enrichment analysis (GSEA) was completed by a SetRank method (PMID: 28259142). The heatmaps and Venn Diagrams were generated in R (package v3.4.0). The heatmaps were generated from FPKM values of the genes that were considered significant compared to the 19% protein group. For each heatmap, the red, white, and blue colors indicate higher than mean, close to mean, and lower than mean expression of a particular gene, respectively, as measured by the row of standardized Z-scores. The rows are organized by hierarchical clustering using agglomerative clustering with complete linkage and Euclidian distance metric. The volcano plot and Venn diagrams were constructed by a Pearson calculation with the top 2.5% of genes in either direction considered significant. All genetic data are available at the online database GEO: GSE111778.

Protein isolation—Whole frozen hippocampus was homogenized using the bead method for 50hz for 30 s (QIAGEN TissueLyser LT) in 500 μL ice-cold RIPA buffer containing Tris-

HCl, NaCl, Triton X-100, Na-deoxycholate, SDS, and fresh protease and phosphatase inhibitor tablets (Roche cOmplete, EDTA-free Protease Inhibitor Cocktail). The tissue was let to sit on ice for 10 minutes followed by 20 minutes of centrifugation at 14,000 rpm. The supernatant was transferred to a fresh ice-cold tube and protein concentrations were assessed using a bicinchoninic acid (BCA) assay (Thermo Scientific, Pierce BCA Protein Assay Kit). Samples were then diluted to approximately the same concentrations before being stored at minus 80°C until further analysis. Protein lysates were used for subsequent enzymatic activity assays, Milliplex Map Panels, and western blots.

Western blots—Lysates were prepared for bis/tris polyacrylamide gel electrophoresis under reduced conditions. Proteins were transferred to nitrocellulose membranes (Invitrogen) and immediately stained with Ponceau S dye (Sigma Aldrich, St. Louis, MO, USA) for rapid and reversible visualization of total protein per lane. Protein expression was detected using specific primary antibodies. Antibodies raised against p-MTOR (#2971; 1:000), MTOR (#2983; 1:1000), SIRT1 (#9475; 1:750), and β-ACTIN (#4970; 1:1000) were purchased from Cell Signaling Technology (Danvers, MA, USA). Antibodies raised against DREBRIN (ab60933; 1:000), GAPDH (ab9485; 1:1000), and PGC1-α (ab54481; 1:1000) were purchased from abcam (Cambridge, UK). All antibodies were detected using secondary rabbit IgG-horse radish peroxidase (#7074; 1:5000) purchased from Cell-Signaling and visualized by enhanced chemiluminescence (GE Healthcare, Chicago, IL, USA). Levels of specific proteins were normalized to total protein as visualized to ponceau S staining (Eaton et al., 2013) and band densitometric values analyzed with ImageJ (National Institutes of Health, Bethesda, MD). Loading controls GAPDH and ACTIN bands are shown along with their representative blots solely for comparison purposes.

Milliplex map panel enzymatic activity assays—Levels of IL-6, IL-10, and TNFa were assessed using the mouse cytokine/chemokine magnetic bead panel 96-Well Plate Assay (Cat # MCYTOMAG – 70K, EMD Millipore Corporation, Billerica, MA, USA) per manufacturer's instructions. After a plate wash, 25ul of each standard or control was added to the appropriate wells followed by 25 μL of assay buffer to the sample wells. 25 μL of whole hippocampal tissue lysates were added to the appropriate wells followed by 25 μL of premixed cytokine panel beads. The plate was sealed, covered with aluminum foil, and incubated overnight at 4°C. The following day the plate was removed from 4°C and washed 2 times with the provided wash buffer. 25 μL of detection antibodies were added to each well and the plate was covered with foil and incubated with shaking for 1 hour at RT. 25 μL of Streptavidin-Phycoerythrin was then added to each well, covered with foil, and incubated with shaking for 30 minutes. The plate was then washed 2 times and 150 μL of the provided drive fluid was added to each well followed by 5 minutes of shaking. The plate was run and read on MAGPIX® machine with xPonenent® Software (EMD Millipore Corporation, Billerica, MA, USA). The data were analyzed using Xponent® software. Briefly, the software analyzed median fluorescent intensity data using 5-parameter logistic or spline curve-fitting method for calculating each cytokine concentration in samples. Data are presented as ng/mg protein.

BDNF enzymatic activity assay—The BDNF ImmunoAssay Elisa was performed per manufacturer's instructions (Promega Corporation, Madison, WI, USA). Flat-bottom 96-well plates were coated with Anti-BDNF Monoclonal Antibody overnight at 4°C to bind soluble antibody. After the addition of 25 μL of each standard or lysate, the plate was incubated for 2 hours and secondary antibody was added. The plate was washed 3 times with TBS-T and the amount of bound pAb was detected using an anti-IgY horseradish peroxidase antibody. Unbound conjugate was removed by washing 5 times with TBST, a chomogenic substrate was added, and color was measured on a spectrometer at a wavelength of 450nm. Data are presented as mg BDNF/mg protein.

Golgi Staining—A rapid Golgi Stain was performed per manufacturer's instructions (FD Neurotechnologies, Inc, Columbia, MD, USA). Brains were removed and rinsed with ice-cold double deionized water. The complete right section was submerged in an impregnation solution consisting of equal parts of solution 'A' and solution 'B'. Samples were stored at room temperature in the dark for 2 weeks and then moved to solution 'C' for 3 days. They were then cut on the midsagittal plane with a vibratome at 100 mm to visualize and quantify dendritic spines (Zaqout and Kaindl, 2016). Samples were left to dry before the staining protocol. Sections were rinsed in distilled water before placing into a mixture consisting of 1 part solution 'D' and 1 part solution 'E'. After an additional rinse, sections were dehydrated in increasing 50%, 75%, and 95% ethanol solutions before clearing in xylene and coverslipping in DPX mounting media for histology (Sigma Aldrich, St. Louis, MO, USA).

Dendritic spine quantification—Slides were imaged on an Olympus VS-120 Slide Scanner at 40X magnification which gave good resolution for spine counting purposes (Orlowski and Bjarkam, 2012). 25 z-slices of 1 mm each were imaged from each hippocampus. Dendritic spines were quantified using NeuronStudio software (Mount Sanai School of Medicine, available at http://research.mssm.edu/cnic/tools-ns.html) and blindly counted (DW). It has been demonstrated that the manual counting method by an investigator does not produce significantly different results when compared to other software or semi-automatic counting methods (Orlowski and Bjarkam, 2012). Spines were quantified in the dentate gyrus of each hippocampus and secondary and tertiary branches of each neuron were analyzed. A total of 8 – 12 segments were quantified from each hippocampus depending on the quality of the stain. The quantified dendritic branch segments were required to have the characteristics as previously described (Jacobs et al., 2014): (1) completely and darkly stained near the center of the 100 mm section, (2) contain no broken sections with complete spines, and (3) isolated without interference or overlap from other structures. Data are presented at the number of spines per 10 microns (Stranahan et al., 2009).

Immunofluorescence—Brains were carefully removed and cut on a midsagittal plane. The left side was placed in 4% formalin for 24 hours followed by 30% sucrose cryoprotection for 24 hours at 4°C. Brains were embedded in OCT (Siltera-Finetele, Inc, USA, Torrance, CA) before slowly freezing on dry ice and storing at —80°C until further use. They were sliced at 30 mm on a midsagittal plane on a cryostat. 5 sections were taken from each brain and mounted on slides. For Iba1 staining, sections were post-fixed with 4% PFA before quenching with 50 mM NH_4CL. For antigen retrieval, a commercially available

Proteinase K solution was used for three minutes (Sigma Aldrich, St. Louis, MO, USA) and tissue was blocked for 30 minutes with 10% goat serum in PBS. Slides were incubated with primary antibodies Iba1 (1:250; GeneTex Irvine, CA, USA) overnight at 4°C. Sections were thoroughly washed and incubated with the fluorescent secondary antibody (1:1000, Cyanine 3, ThermoFisher Scientific) for 1 hour before washing and coverslipping with vectashield mounting media containing DAPI (Vector Laboratories, Burlingame, CA, USA). For GFAP, slides were washed with PBST before blocking for 30 minutes in 3% goat serum in PBS. Slides were placed into primary antibody (1:2000, abcam, United States) diluted in 3% goat serum in PBS. Slides were incubated overnight at 4 degrees followed by washing with PBST and a 1 hour incubation in secondary antibody (1:1000; Cyanine3, ThermoFisher Scientific) for one hour. Slides were imaged on a on an Olympus VS-120 Slide Scanner at 20X magnification (Iba1) or a Leica confocal microscope with white light laser (WLL), coupled with a 20X HC PL APO CS2 NA 0.75 lens (GFAP). Images were quantified using ImageJ. Data are presented as the number of $Iba1^+$ cells per $1mm^2$ in the hippocampus or the mean corrected total hippocampus fluorescence (GFAP).

Behavioral testing—Animals were handled extensively before and during the testing phase to acclimatize them to human interaction and minimize potential anxiety caused by interference. Mice received a minimum 2-hours of room habituation before commencing each test. Animals were tested in random order during each testing period and equipment was thoroughly cleaned with 80% ethanol between trials to minimize scents. To test memory during aging animal performance was assessed on both the Novel Object Recognition and Barnes Maze memory tasks. The same animals were tested at young and old age in a longitudinal manner, similar to human dementia and memory studies (Tian et al., 2017). The two-time points were 13 months of age (young) and 23 months of age (old). Animals received a minimum 3 days rest in between the two tests. Male and female results were analyzed separately because of innate behavioral and response differences between sexes (Simpson and Kelly, 2012).

Novel Object Recognition (NOR)—The NOR task was performed in a custom made white opaque plexiglass box (40cmx40cmx40cm; City West Plastic, Sydney, NSW). The task was performed as previously described (Bevins and Besheer, 2006) with an inter-trial interval of 24 hours. On day 1, mice were placed into the box and allowed to explore (habituation period) for 5 minutes followed by one hour of rest before the first trial. Two identical non-toxic and odourless objects (cell culture flasks filled with sand) were placed into the box (5cm from each wall) and the mice could explore for 5 minutes. After an inter-trial interval of 24 hours the mice were placed back into the box but one of the old objects was replaced with a new one (tower of Legos blocks) of similar shape, size, and height. The trial ended once a total exploration time of 20 s was reached, or 5 minutes elapsed. A recognition index (RI) was calculated as the time the mouse spent exploring the new object over total object exploration time. Mice were excluded from the analysis if they did not reach the 5-minute exploration criteria. All trials were recorded with an Any Maze USB camera at 30 frames per second and quantified with a stopwatch by two independent and skilled reviewers.

Barnes Maze (BM)—The Barnes maze task was performed as previously described (Sunyer et al., 2007). An opaque plastic maze was constructed (100 cm in diameter; City West Plastics, Sydney, NSW) with 20 equally-spaced concentric holes around the perimeter. A black escape box was placed in a random location under one of the holes. Distinct spatial cues (large cut-outs of black shapes – a circle, square, and triangle) were placed on walls around the room and the location of the cues remained constant throughout the testing period. Training on day one consisted of gently guiding the mouse to the escape box and covering it in the dark for one minute. Testing consisted of 4 trials (3 minutes maximum) per day, per mouse, for 4 days in a row. If the mouse could not find the hole after three minutes, it was gently guided there. After each trial completion, the hole was covered in the dark for one minute. All videos were recorded with an AnyMaze USB camera at 30 frames/second and data were analyzed using AnyMaze (Stoelting, Wood Dale, IL, USA) and GraphPad Prism 7. Data are represented as the mean ± SEM in seconds taken to completely enter the escape box from the start of the trial.

QUANTIFICATION AND STATISTICAL ANALYSIS

Statistical parameters, significance, and the exact n (number of animals) values are reported in the figure legends. Metabolic measures, immunoblotting, and behavioral data were separated by sex. Male and female mice were combined for biological replicates in the other analyses because there were no statistically significant differences between sexes. Data were analyzed with Excel, R-studio, and GraphPad Prism 7 (La Jolla, CA, USA). The BM data were analyzed using 2 - way ANOVA (treatment x trial time) with repeated-measures (day) and an ANOVA was used to calculate differences among the groups on individual days. All other data were analyzed by an analysis of variance (ANOVA) with diet treatment as a factor for parametric data followed by a Tukey multiple comparison test with a single pooled variance. For non-parametric data, a Kruskal-Wallis ANOVA was used followed by a Dunn's post hoc multiple comparison test. Linear regression was used to determine relationships between variables and a Pearson's correlation was used to calculate statistically significant relationships. Data are represented as means ± SEM and p values of less than 0.05 were considered statistically significant.

DATA SOFTWARE AND AVAILABILITY

The accession number for the RNA sequencing data reported in this paper is GEO: GSE111778.

Supplementary Material

Refer to Web version on PubMed Central for supplementary material.

ACKNOWLEDGMENTS

REFERENCES

Alavi MS, Shamsizadeh A, Azhdari-Zarmehri H, and Roohbakhsh A (2018). Orphan G protein-coupled receptors: the role in CNS disorders. Biomed. Pharmacother 98, 222–232. [PubMed: 29268243]

Beste C, Ocklenburg S, von der Hagen M, and Di Donato N (2016). Mammalian cadherins DCHS1-FAT4 affect functional cerebral architecture. Brain Struct. Funct 221, 2487–2491. [PubMed: 25930014]

Bevins RA, and Besheer J (2006). Object recognition in rats and mice: a one-trial non-matching-to-sample learning task to study 'recognition memory'. Nat. Protoc 1, 1306–1311. [PubMed: 17406415]

Brahmachari S, Fung YK, and Pahan K (2006). Induction of glial fibrillary acidic protein expression in astrocytes by nitric oxide. J. Neurosci 26, 4930–4939. [PubMed: 16672668]

Buffa R, Mereu E, Putzu P, Mereu RM, and Marini E (2014). Lower lean mass and higher percent fat mass in patients with Alzheimer's disease. Exp. Gerontol 58, 30–33. [PubMed: 25019474]

Cheng Y, Cawley NX, and Loh YP (2014). Carboxypeptidase E (NF-α1): a new trophic factor in neuroprotection. Neurosci. Bull 30, 692–696. [PubMed: 24691800]

Dye L, Boyle NB, Champ C, and Lawton C (2017). The relationship between obesity and cognitive health and decline. Proc. Nutr. Soc 76, 443–454. [PubMed: 28889822]

Eaton SL, Roche SL, Llavero Hurtado M, Oldknow KJ, Farquharson C, Gillingwater TH, and Wishart TM (2013). Total protein analysis as a reliable loading control for quantitative fluorescent Western blotting. PLoS ONE 8, e72457. [PubMed: 24023619]

Garcia JM, Stillings SA, Leclerc JL, Phillips H, Edwards NJ, Robicsek SA, Hoh BL, Blackburn S, and Doré S (2017). Role of interleukin-10 in acute brain injuries. Front. Neurol 8, 244. [PubMed: 28659854]

Gewurz BE, Towfic F, Mar JC, Shinners NP, Takasaki K, Zhao B, Cahir-McFarland ED, Quackenbush J, Xavier RJ, and Kieff E (2012). Genome-wide siRNA screen for mediators of NF-kB activation. Proc. Natl. Acad. Sci. USA 109, 2467–2472. [PubMed: 22308454]

Hadem IKH, Majaw T, Kharbuli B, and Sharma R (2017). Beneficial effects of dietary restriction in aging brain. J. Chem. Neuroanat Published online October 12, 2017. 10.1016/j.jchemneu.2017.10.001.

Ingram DK, Weindruch R, Spangler EL, Freeman JR, and Walford RL (1987). Dietary restriction benefits learning and motor performance of aged mice. J. Gerontol 42, 78–81. [PubMed: 3794202]

Jacobs B, Johnson NL, Wahl D, Schall M, Maseko BC, Lewandowski A, Raghanti MA, Wicinski B, Butti C, Hopkins WD, et al. (2014). Comparative neuronal morphology of the cerebellar cortex in afrotherians, carnivores, cetartiodactyls, and primates. Front. Neuroanat 8, 24. [PubMed: 24795574]

Kesner RP (2018). An analysis of dentate gyrus function (an update). Behav. Brain Res 354, 84–91, Published online July 26, 2017. 10.1016/j.bbr.2017.07.033. [PubMed: 28756212]

Kim YN, Jung HY, Eum WS, Kim DW, Shin MJ, Ahn EH, Kim SJ, Lee CH, Yong JI, Ryu EJ, et al. (2014). Neuroprotective effects of PEP-1-carbonyl reductase 1 against oxidative-stress-induced ischemic neuronal cell damage. Free Radic. Biol. Med 69, 181–196. [PubMed: 24440593]

Le Couteur DG, Solon-Biet S, Cogger VC, Mitchell SJ, Senior A, de Cabo R, Raubenheimer D, and Simpson SJ (2016). The impact of low-protein high-carbohydrate diets on aging and lifespan. Cell. Mol. Life Sci 73, 1237–1252. [PubMed: 26718486]

Mattson MP (2010). The impact of dietary energy intake on cognitive aging. Front. Aging Neurosci 2, 5. [PubMed: 20552045]

Mattson MP, Moehl K, Ghena N, Schmaedick M, and Cheng A (2018). Intermittent metabolic switching, neuroplasticity and brain health. Nat. Rev. Neurosci 19, 63–80.

Mazucanti CH, Cabral-Costa JV, Vasconcelos AR, Andreotti DZ, Scavone C, and Kawamoto EM (2015). Longevity pathways (mTOR, SIRT, Insulin/IGF-1) as key modulatory targets on aging and neurodegeneration. Curr. Top. Med. Chem 15, 2116–2138. [PubMed: 26059361]

Mitchell SJ, Madrigal-Matute J, Scheibye-Knudsen M, Fang E, Aon M, González-Reyes JA, Cortassa S, Kaushik S, Gonzalez-Freire M, Patel B, et al. (2016). Effects of sex, strain, and energy intake on hallmarks of aging in mice. Cell Metab 23, 1093–1112. [PubMed: 27304509]

Newman JC, Covarrubias AJ, Zhao M, Yu X, Gut P, Ng CP, Huang Y, Haldar S, and Verdin E (2017). Ketogenic diet reduces midlife mortality and improves memory in aging mice. Cell Metab 26, 547–557.e8. [PubMed: 28877458]

Nikonova EV, Gilliland JD, Tanis KQ, Podtelezhnikov AA, Rigby AM, Galante RJ, Finney EM, Stone DJ, Renger JJ, Pack AI, et al. (2017). Transcriptional profiling of cholinergic neurons from basal forebrain identifies changes in expression of genes between sleep and wake. Sleep 40 10.1093/sleep/zsx059.

Orlowski D, and Bjarkam CR (2012). A simple reproducible and time saving method of semi-automatic dendrite spine density estimation compared to manual spine counting. J. Neurosci. Methods 208, 128–133. [PubMed: 22595026]

Pani G (2015). Neuroprotective effects of dietary restriction: evidence and mechanisms. Semin. Cell Dev. Biol 40, 106–114. [PubMed: 25773162]

Paradis S, Harrar DB, Lin Y, Koon AC, Hauser JL, Griffith EC, Zhu L, Brass LF, Chen C, and Greenberg ME (2007). An RNAi-based approach identifies molecules required for glutamatergic and GABAergic synapse development. Neuron 53, 217–232. [PubMed: 17224404]

Parrella E, Maxim T, Maialetti F, Zhang L, Wan J, Wei M, Cohen P, Fontana L, and Longo VD (2013). Protein restriction cycles reduce IGF-1 and phosphorylated Tau, and improve behavioral performance in an Alzheimer's disease mouse model. Aging Cell 12, 257–268. [PubMed: 23362919]

Plank M, Wuttke D, van Dam S, Clarke SA, and de Magalhães JP (2012). A meta-analysis of caloric restriction gene expression profiles to infer common signatures and regulatory mechanisms. Mol. Biosyst 8, 1339–1349. [PubMed: 22327899]

Prolla TA, and Mattson MP (2001). Molecular mechanisms of brain aging and neurodegenerative disorders: lessons from dietary restriction. Trends Neurosci 24 (11, Suppl), S21–S31. [PubMed: 11881742]

Ren H, Orozco IJ, Su Y, Suyama S, Gutie´ rrez-Jua´ rez R, Horvath TL, Wardlaw SL, Plum L, Arancio O, and Accili D (2012). FoxO1 target Gpr17 activates AgRP neurons to regulate food intake. Cell 149, 1314–1326. [PubMed: 22682251]

Schafer MJ, Dolgalev I, Alldred MJ, Heguy A, and Ginsberg SD (2015). Calorie restriction suppresses age-dependent hippocampal transcriptional signatures. PLoS ONE 10, e0133923. [PubMed: 26221964]

Simpson J, and Kelly JP (2012). An investigation of whether there are sex differences in certain behavioural and neurochemical parameters in the rat. Behav. Brain Res 229, 289–300. [PubMed: 22230114]

Simpson SJ, Le Couteur DG, Raubenheimer D, Solon-Biet SM, Cooney GJ, Cogger VC, and Fontana L (2017). Dietary protein, aging and nutritional geometry. Ageing Res. Rev 39, 78–86. [PubMed: 28274839]

Simpson SJ, and Raubenheimer D (2012). The Nature of Nutrition: A Unifying Framework from Animal Nutrition to Human Obesity (Princeton University Press).

Solon-Biet SM, McMahon AC, Ballard JW, Ruohonen K, Wu LE, Cogger VC, Warren A, Huang X, Pichaud N, Melvin RG, et al. (2014). The ratio of macronutrients, not caloric intake, dictates cardiometabolic health, aging, and longevity in ad libitum-fed mice. Cell Metab 19, 418–430. [PubMed: 24606899]

Solon-Biet SM, Mitchell SJ, Coogan SC, Cogger VC, Gokarn R, McMahon AC, Raubenheimer D, de Cabo R, Simpson SJ, and Le Couteur DG (2015). Dietary protein to carbohydrate ratio and caloric restriction: comparing metabolic outcomes in mice. Cell Rep 11, 1529–1534. [PubMed: 26027933]

Solon-Biet SM, Cogger VC, Pulpitel T, Heblinski M, Wahl D, McMahon AC, Warren A, Durrant-Whyte J, Walters KA, Krycer JR, et al. (2016). Defining the nutritional and metabolic context of FGF21 using the Geometric Framework. Cell Metab 24, 555–565. [PubMed: 27693377]

Sørensen A, Mayntz D, Raubenheimer D, and Simpson SJ (2008). Protein-leverage in mice: the geometry of macronutrient balancing and consequences for fat deposition. Obesity (Silver Spring) 16, 566–571. [PubMed: 18239565]

Stranahan AM, Lee K, Martin B, Maudsley S, Golden E, Cutler RG, and Mattson MP (2009). Voluntary exercise and caloric restriction enhance hippocampal dendritic spine density and BDNF levels in diabetic mice. Hippo-campus 19, 951–961.

Sunyer B, Patil S, Hö ger H, and Lubec G (2007). Barnes maze, a useful task to assess spatial reference memory in the mice. Nature, Published online October 4, 2007. 10.1038/nprot.2007.390.

Testa G, Biasi F, Poli G, and Chiarpotto E (2014). Calorie restriction and dietary restriction mimetics: a strategy for improving healthy aging and longevity. Curr. Pharm. Des 20, 2950–2977. [PubMed: 24079773]

Tian Q, An Y, Resnick SM, and Studenski S (2017). The relative temporal sequence of decline in mobility and cognition among initially unimpaired older adults: results from the Baltimore Longitudinal Study of Aging. Age Ageing 46, 445–451. [PubMed: 27744302]

Toda T, and Gage FH (2017). Review: adult neurogenesis contributes to hippocampal plasticity. Cell Tissue Res 373, 693–709. [PubMed: 29185071]

Tolppanen AM, Ngandu T, Kåreholt I, Laatikainen T, Rusanen M, Soininen H, and Kivipelto M (2014). Midlife and late-life body mass index and late-life dementia: results from a prospective population-based cohort.J. Alzheimers Dis 38, 201–209. [PubMed: 23948937]

Valencak TG, Osterrieder A, and Schulz TJ (2017). Sex matters: The effects of biological sex on adipose tissue biology and energy metabolism. Redox Biol 12, 806–813. [PubMed: 28441629]

Wahl D, Cogger VC, Solon-Biet SM, Waern RV, Gokarn R, Pulpitel T, Cabo Rd., Mattson MP, Raubenheimer D, Simpson SJ, and Le Couteur DG (2016). Nutritional strategies to optimise cognitive function in the aging brain. Ageing Res. Rev 31, 80–92. [PubMed: 27355990]

Wahl D, Coogan SC, Solon-Biet SM, de Cabo R, Haran JB, Raubenheimer D, Cogger VC, Mattson MP, Simpson SJ, and Le Couteur DG (2017). Cognitive and behavioral evaluation of nutritional interventions in rodent models of brain aging and dementia. Clin. Interv. Aging 12, 1419–1428. [PubMed: 28932108]

Walker DG, Whetzel AM, and Lue LF (2015). Expression of suppressor of cytokine signaling genes in human elderly and Alzheimer's disease brains and human microglia. Neuroscience 302, 121–137. [PubMed: 25286386]

Willette AA, Coe CL, Birdsill AC, Bendlin BB, Colman RJ, Alexander AL, Allison DB, Weindruch RH, and Johnson SC (2013). Interleukin-8 and interleukin-10, brain volume and microstructure, and the influence of calorie restriction in old rhesus macaques. Age (Dordr.) 35, 2215–2227. [PubMed: 23463321]

Wood SH, van Dam S, Craig T, Tacutu R, O'Toole A, Merry BJ, and de Magalhães JP (2015). Transcriptome analysis in calorie-restricted rats implicates epigenetic and post-translational mechanisms in neuroprotection and aging. Genome Biol 16, 285. [PubMed: 26694192]

Zaqout S, and Kaindl AM (2016). Golgi-Cox staining step by step. Front. Neuroanat 10, 38. [PubMed: 27065817]

Zeier Z, Madorsky I, Xu Y, Ogle WO, Notterpek L, and Foster TC (2011). Gene expression in the hippocampus: regionally specific effects of aging and caloric restriction. Mech. Ageing Dev 132, 8–19. [PubMed: 21055414]

Zhang B, Bailey WM, Braun KJ, and Gensel JC (2015). Age decreases macrophage IL-10 expression: Implications for functional recovery and tissue repair in spinal cord injury. Exp. Neurol 273, 83–91. [PubMed: 26263843]

Highlights

- Calorie restriction (CR) and low-protein, high-carb (LPHC) diets improve health

- Hippocampus RNA expression is positively influenced by CR and LPHC diets

- Nutrient-sensing pathways are similarly influenced by CR and LPHC diets

- CR and LPHC diets positively influence dendritic spines and cognitive function
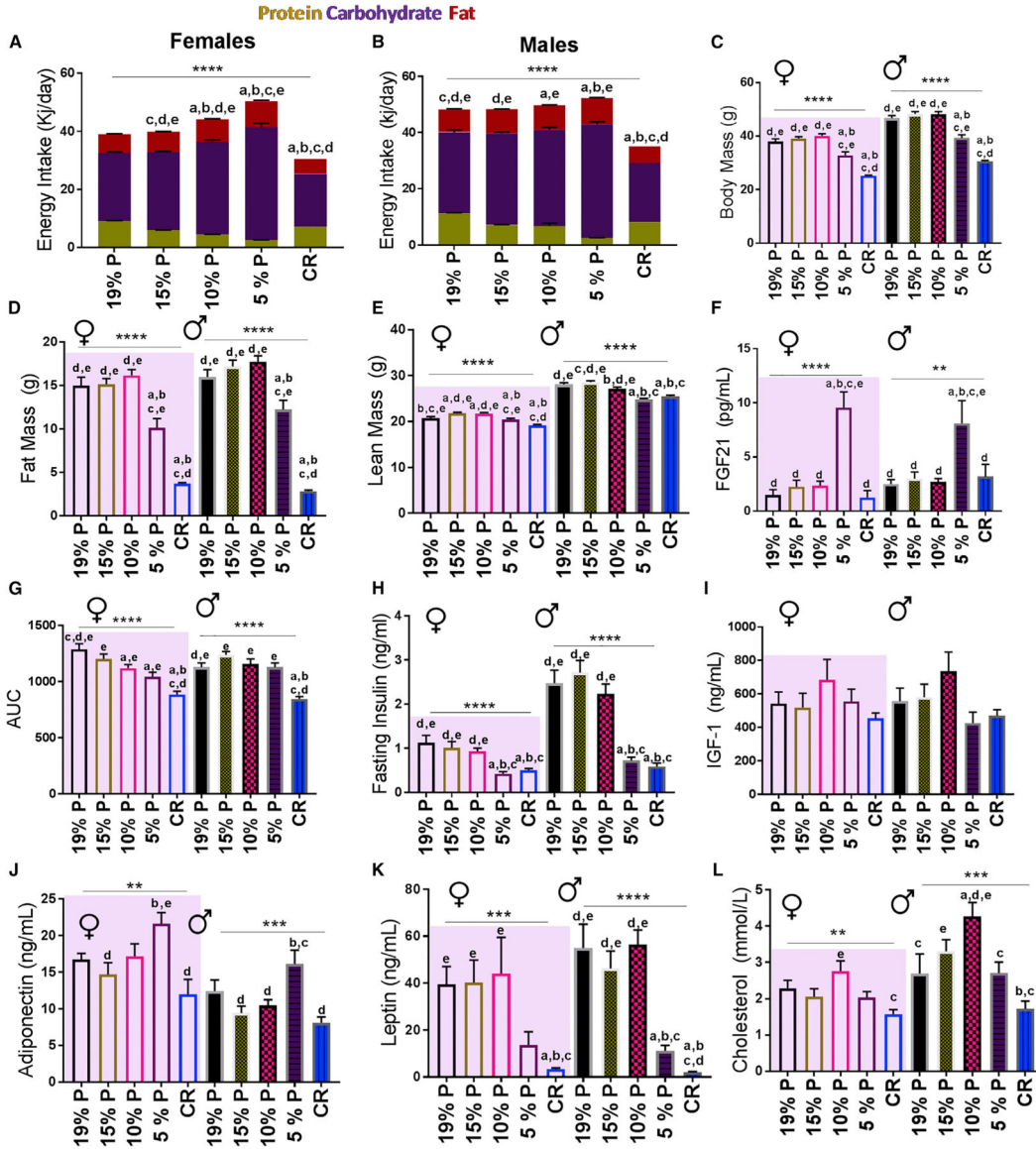
Figure 1. Impact of CR and LPHC Diets on Cardiometabolic Health in Male and Female 15-Month-Old Mice

(A)Female daily energy intake (kJ/day) by macronutrient.

(B)Male daily energy intake (kJ/day) by macronutrient.

(C)Body mass of mice. n = 25–30 mice per group.

(D)Total fat mass. n = 25–35 mice per experimental group.

(E)Total lean mass. n = 25–35 mice per experimental group.

(F)Serum FGF-21. n = 10–12 mice per experimental group.

(G)Glucose tolerance test (area under the curve, AUC). n = 20–30 mice per group.

(H)Fasted serum insulin. n = 20–30 mice per group.

(I)Serum IGF-1. n = 10–12 mice per group.

(J)Serum adiponectin. n = 10–12 mice per group.

(K)Serum leptin. n = 10–12 mice per group.

(L)Serum cholesterol. n = 10–12 mice per experimental group.

*p < 0.05; **p < 0.01; ***p < 0.001; ****p < 0.0001 ANOVA analysis. a = significantly different to 19% P; b = significantly different to 15% P; c = significantly different to 10% P; d = significantly different to 5% P; e = significantly different to CR as determined by a Tukey's post hoc analysis. Mean ± SEM, See also Table S1.
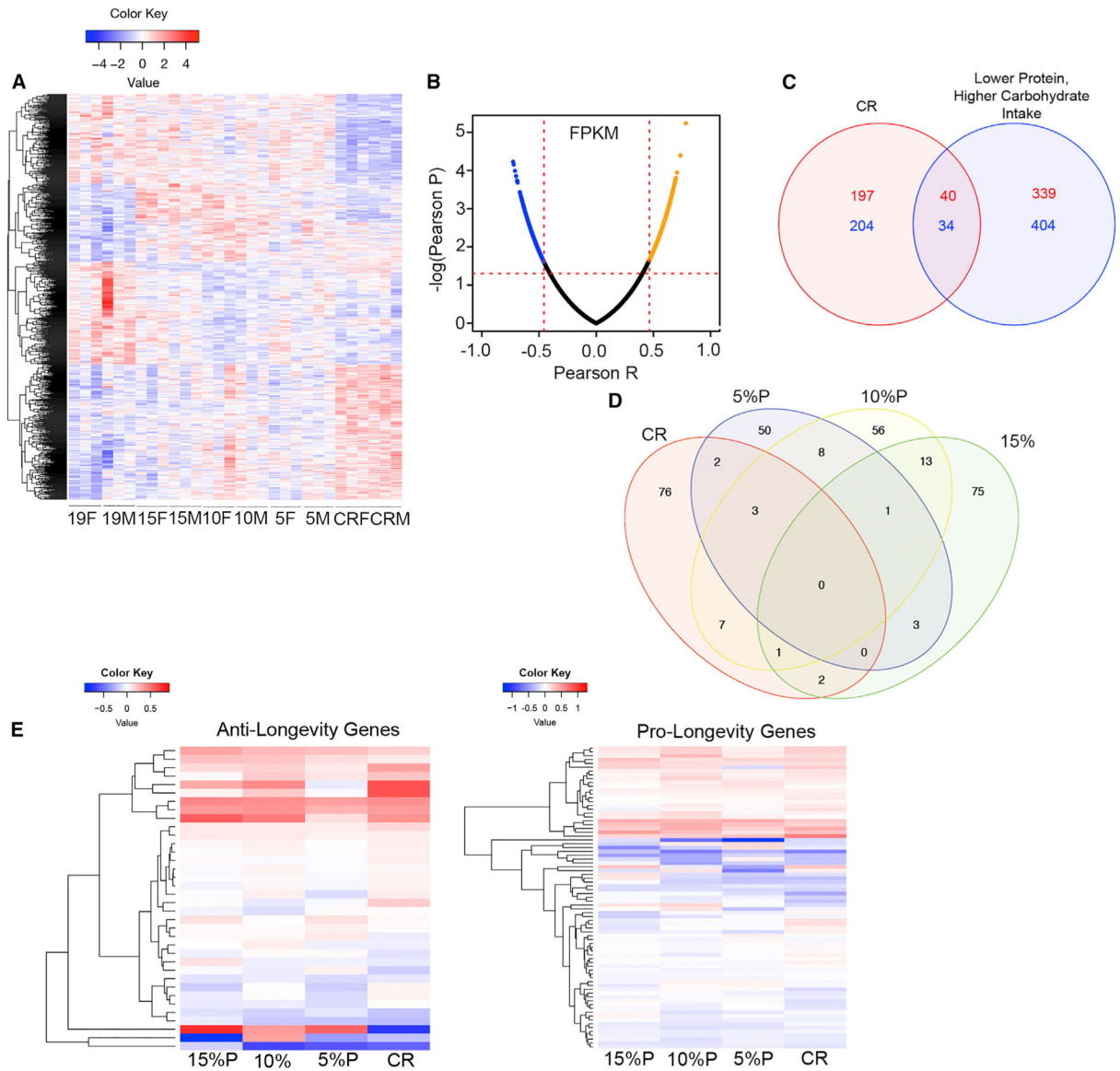
Figure 2. Impact of CR and LPHC Diets on Hippocampal Gene Expression in Male and in Female 15-Month-Old Mice

(A)Heatmap of upregulated or downregulated genes compared to average expression across all genes as measured by the row of standardized Z scores. n = 3 mice per experimental group.

(B)Volcano plot of the top 5% of genes positively correlated or negatively correlated with daily protein intake. n = 3 mice per experimental group.

(C)Venn diagram showing genes upregulated (red) or downregulated (blue) by CR when compared to control 19% protein diet and genes overexpressed with lower protein intake (red) and underexpressed with lower protein intake (blue) as measured by a Pearson correlation.

(D)Venn diagram of total differentiated biological processes among the groups. Each group was compared to control 19% protein diet. n = 6 biological replicates per group.

(E)Heatmap of significantly upregulated or downregulated genes identified by GenAge as anti-longevity genes. Each experimental group is compared to control 19% protein diet, and the degree of relatedness among the genes is shown on the y axis. n = 6 replicates per group.

(F)Heatmap of significantly upregulated or downregulated genes identified by GenAge as pro-longevity genes. Each group is compared to control 19% protein diets, and the degree of relatedness among the genes is shown on the y axis. n = 6 replicates group.

See also Tables S2, S3, S4, S5, S6, and S7.
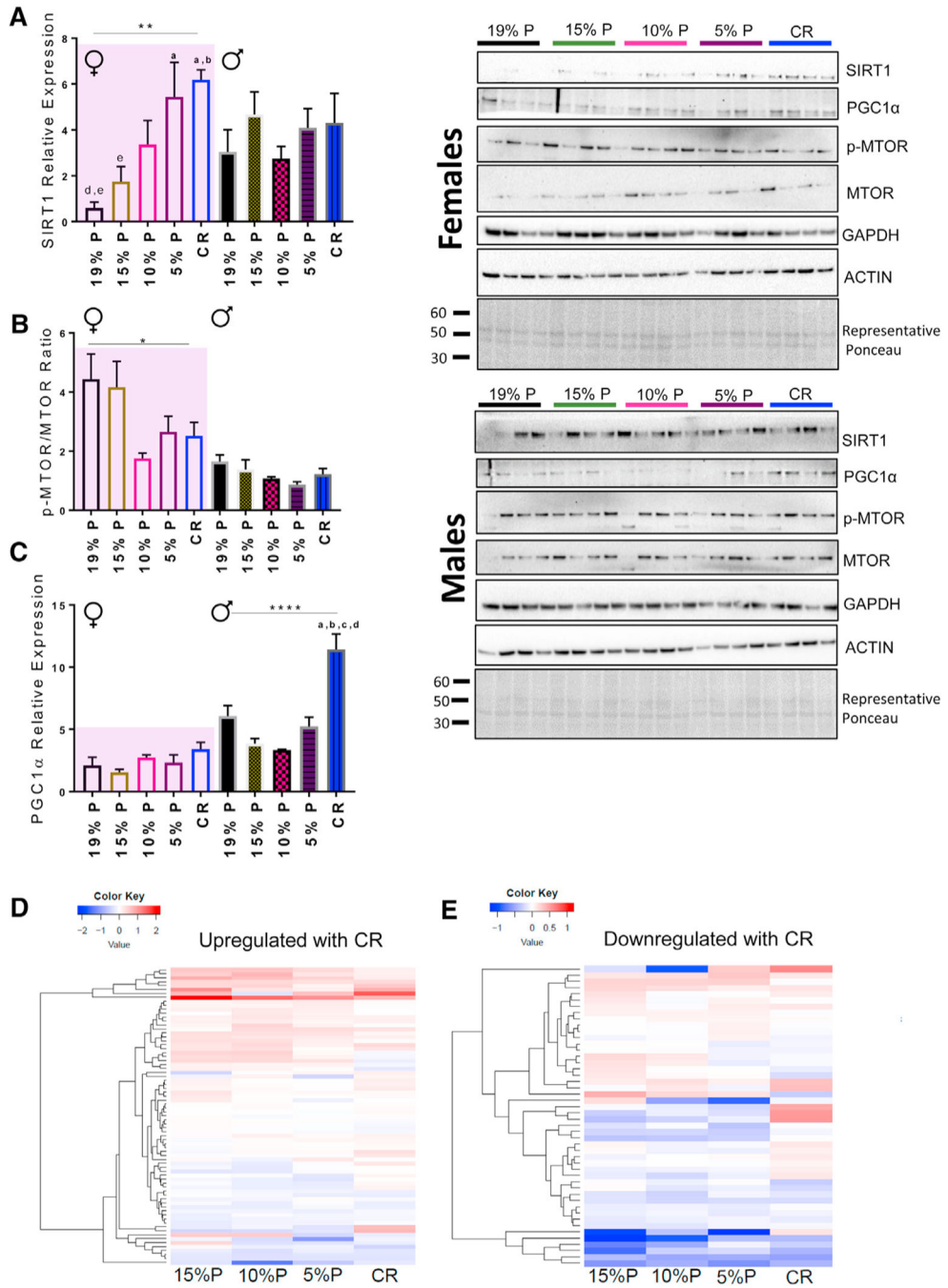
Figure 3. Changes in the Expression of Several Key Nutrient-Sensing Proteins and CR Genes in Response to CR and LPHC Diets at 15 Months of Age

(A) SIRT1 protein expression from whole hippocampus homogenates. n = 4 mice per group.

(B) The ratio of phospho-MTOR:total MTOR expression from whole-hippocampus homogenates. n = 4 mice per group. See also Figure S2.

(C) PGC1-a protein expression from whole hippocampus homogenates. n = 4 per group. Representative Ponceau S staining is shown, and each band was normalized to the total densitometric value for total protein per lane.

(D) Heatmap of genes known to be upregulated with CR. Each group was compared to control 19% protein diets, and the degree of relatedness among the genes is shown on the y axis. n = 6 replicates per group. See also Table S8.

(E) Heatmap of genes known to be downregulated with CR. Each group was compared to control 19% protein diets, and the degree of relatedness among the genes is shown on the y axis. n = 6 replicates per group. See also table S8.

*$p < 0.05$; **$p < 0.01$; ***$p < 0.001$; ****$p < 0.0001$ ANOVA analysis. a = significantly different to 19% P; b = significantly different to 15% P; c = significantly different to 10% P; d = significantly different to 5% P; e = significantly different to CR as determined by a Tukey's post hoc analysis. All data are presented by the mean ± SEM of the biological replicates.
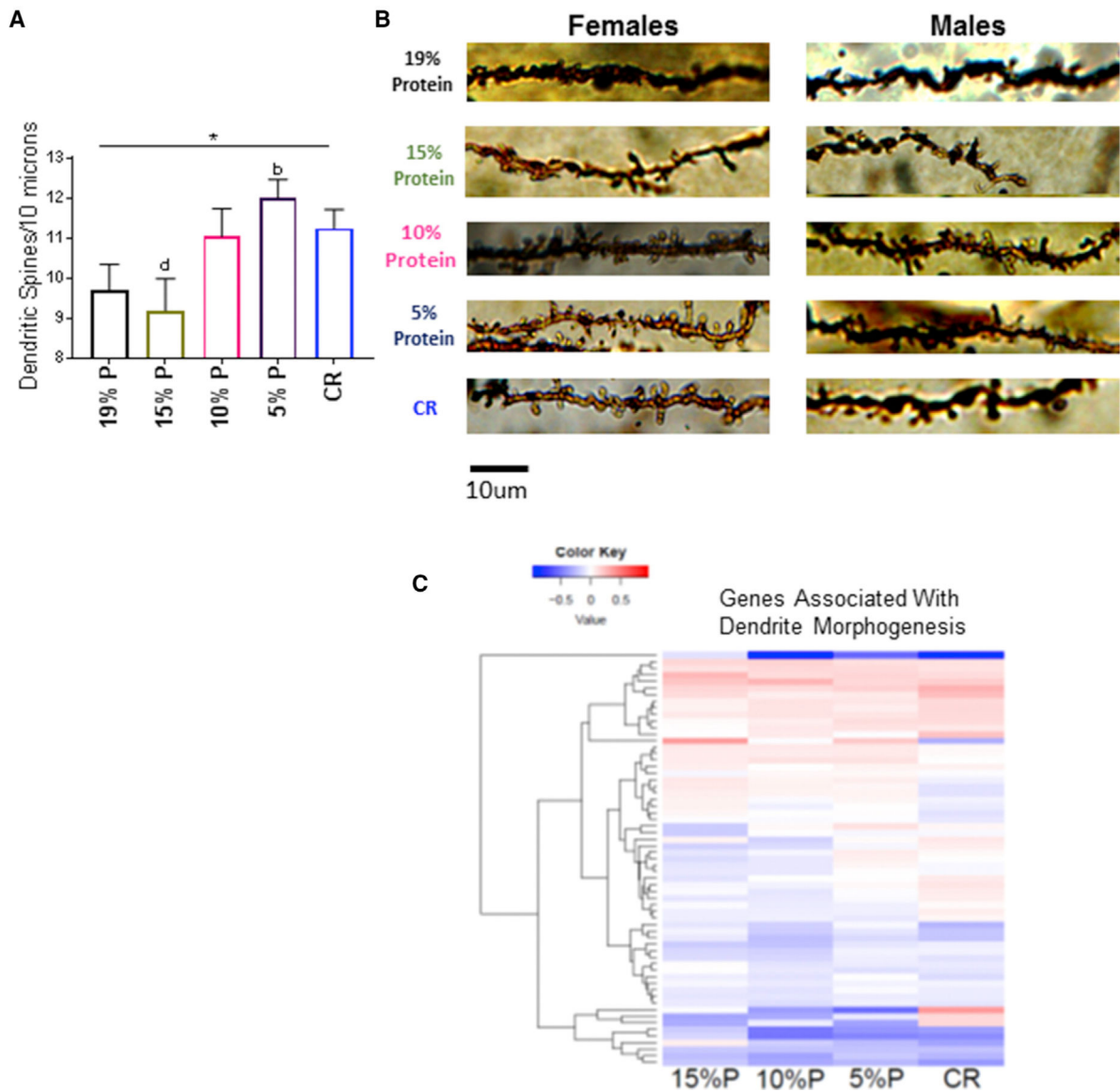
Figure 4. Dendritic Spine Density on Secondary and Tertiary Dendrites in the Hippocampal Dentate Gyrus and Related Genetic Expression at 15 Months of Age

(A)Dendritic spine density of DG neurons. n = 8–12 neurite segments per mouse from each group and 6 – 12 replicates per group depending on the stain quality.

(B)Representative images from dendritic spine segments from each experimental group, 15 months of age. Scale bar, 10 mm. See also Figure S2.

(C)Heatmap of upregulated or downregulated genes that are known to be dendrite morphogenesis. Each group is compared to control 19% protein diets, and the degree of relatedness among the genes is shown on the y axis. n = 6 replicates per group, 15 months of age, 14 months on diet. See also Table S10.

$*p < 0.05$; $**p < 0.01$; $***p < 0.001$; $****p < 0.0001$ ANOVA group analysis. a = significantly different to 19% P; b = significantly different to 15% P; c = significantly different to 10% P; d = significantly different to 5% P; e = significantly different to CR as

determined by a Tukey's post hoc analysis. All data are represented by the mean ± SEM of the biological replicates.
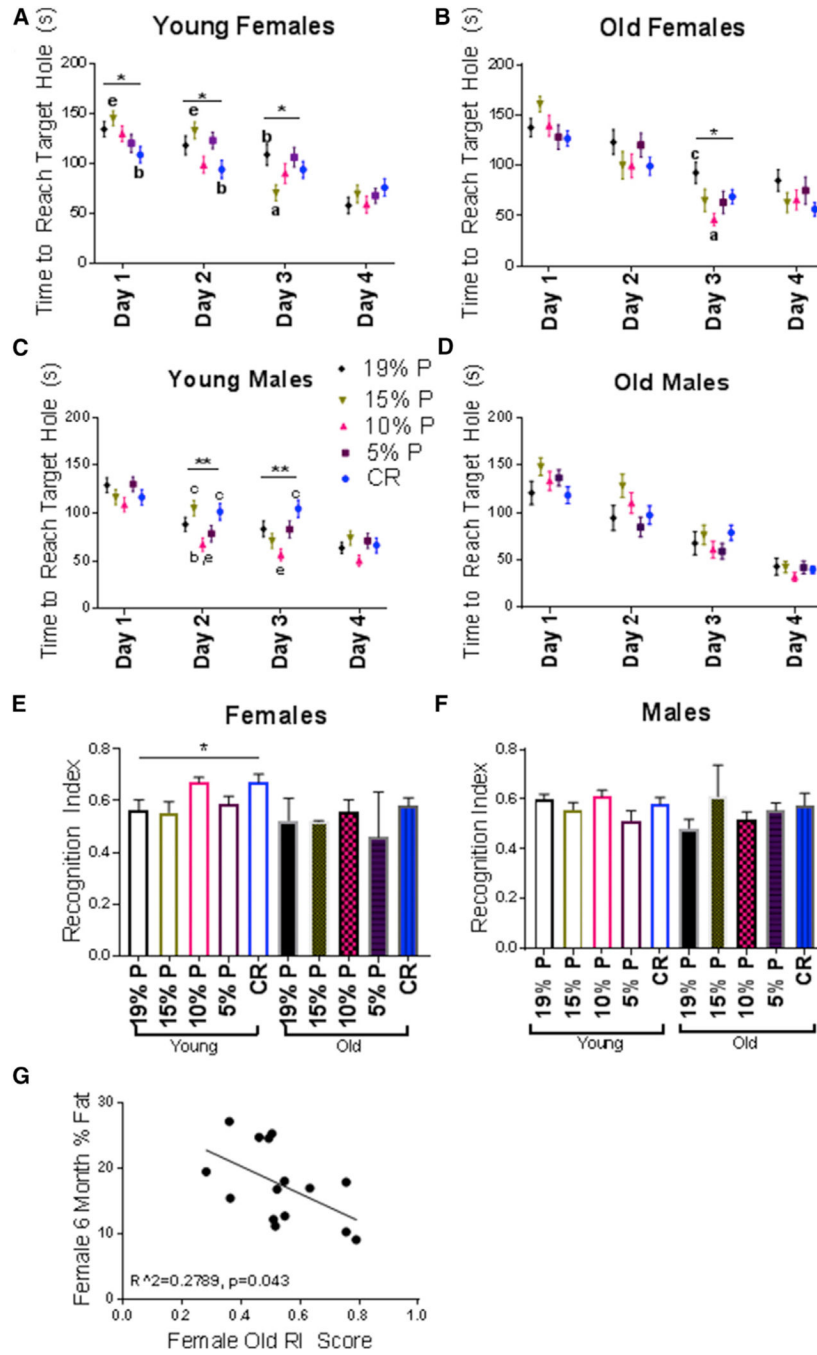
Figure 5. Behavioral and Cognitive Responses to CR and LPHC Diets at 13 and 23 Months of Age

(A) Barnes maze, 13-month-old females. Mean ± SEM of the time to reach the target hole. 4 trials per day, per mouse were completed. n = 12 mice per group.

(B) Barnes maze, 23-month-old females. n = 12 mice per group.

(C) Barnes maze, 13-month-old males. n = 12 mice per group.

(D) Barnes maze, 23-month-old males. n = 5–12 mice per group.

(E) Novel object recognition, 13- and 23-month-old females. Means ± SEM of the recognition index (RI), quantified by a ratio of new object exploration over total object exploration. n = 12 mice per group (young) and n = 5–12 mice per group (old).

(F) Novel object recognition, 13- and 23-month-old males. n = 12 mice per group (young) and n = 5–12 mice per group (old).

(G) Relationship between percent body fat at 6 months and RI score at 23 months, n = 15 females.

*$p < 0.05$; **$p < 0.01$; ***$p < 0.001$; ****$p < 0.0001$ ANOVA group analysis. a = significantly different to 19% P; b = significantly different to 15% P; c = significantly different to 10% P; d = significantly different to 5% P; e = significantly different to CR as determined by a Tukey's post hoc analysis. All data are represented by the mean ± SEM.

REAGENT or RESOURCE	SOURCE	IDENTIFIER
Antibodies		
Phospho-mTOR (Ser2448) Antibody	Cell Signaling Technology	#2971; RRID:AB_330970
mTOR (7C10) Rabbit mAb	Cell Signaling Technology	#2983; RRID:AB_2105622
SirT1 (D1D7) Rabbit mAb	Cell Signaling Technology	#9475; RRID:AB_2617130
β-Actin (13E5) Rabbit mAb	Cell Signaling Technology	#4970; RRID:AB_2223172
Anti-Drebrin antibody	abcam	ab60933; RRID:AB_10675963
Anti-GAPDH antibody - Loading Control	abcam	ab9485; RRID:AB_307275
Anti-PGC1 alpha antibody	abcam	ab54481; RRID:AB_881987
Anti-rabbit IgG, HRP-linked Antibody	Cell Signaling Technology	#7074; RRID:AB_2099233
Rabbit Polyclonal Anti-Iba1 antibody	GeneTex	GTX100042; RRID:AB_1240434
Rabbit Polyclonal Anti-GFAP antibody	Abcam	ab7260; RRID:AB_305808
Goat anit-Rabbit IgG (H+L) Cross-Adsorbed Secondary Antibody, Cyanine3	ThermoFisher Scientific	A10520; RRID:AB_2534029
VECTASHIELD Antifade Mounting Medium with DAPI	Vector Laboratories	H-1200; RRID:AB_2336790
Chemicals, Peptides, and Recombinant Proteins		
DPX Mounting Media for histology	Sigma-Aldrich	06522
cOmplete, EDTA-free Protease Inhibitor Cocktail	Sigma-Aldrich	COEDTAF-RO ROCHE
10x Tris Buffered Saline (TBS)	Bio-Rad	#1706435
TRI Reagent® for DNA, RNA and protein isolation	Sigma-Aldrich	93289
Ponceau S Dye	Sigma-Aldrich	P7170
Critical Commercial Assays		
FD Rapid GolgiStain Kit (large)	FD Neurotechnologies	PK401
BDNF E$_{max}$® ImmunoAssay Systems	Promega	G7610
MCYTOMAG-70K j MILLIPLEX MAP Mouse Cytokine/Chemokine Magnetic Bead Panel - Immunology Multiplex Assay	Merck Millipore	# MCYTOMAG
Pierce BCA Protein Assay Kit	Thermo Fisher Scientific	23225
Mouse Leptin ELISA Kit	Crystal Chem High Performance Assays	90030
Mouse Adiponectin ELISA Kit	Crystal Chem High Performance Assays	80569
Fibroblast Growth Factor 21 Mouse/Rat ELISA	BioVendor Research and Diagnostic Products	RD291108200R
Ultra Sensitive Mouse Insulin ELISA Kit	Crystal Chem High Performance Assays	90080
Deposited Data		
Raw sequence data deposited into NCBI	Total Hippocampus RNA	GEO: GSE111778
Experimental Models: Organisms/Strains		
C57/b6 male and female mice	Animal Resource Centre, Perth, WA	N/A
Software and Algorithms		
NeuronStudio	Mount Sanai School of Medicine, freely	http://research.mssm.edu/cnic/tools-ns.html

REAGENT or RESOURCE	SOURCE	IDENTIFIER
	available available online	
ImageJ	National Institutes of Health, freely available online	https://imagej.nih.gov/ij/
AnyMaze behavioral tracking software	Stoelting Co. Wood Dale, IL.	http://www.anymaze.co.uk/
The R Project for statistical computing	Freely available online	https://www.r-project.org/
GraphPad Prism Software	Available for download online	https://www.graphpad.com/scientific-software/prism/

Table 1.

Diets Used in the Study

Diet	NME (kJ/g)	% Protein NME	% Carbohydrate NME	% Fat NME
CR	14.4	18.8	63.4	17.8
5% protein	14.4	5	77.2	17.8
10% protein	14.4	10	72.2	17.8
15% protein	14.4	15	67.2	17.8
19% protein	14.4	18.8	63.4	17.8

CR, calorie restriction; NME, net metabolizable energy.